COLITIS

C1orf106 is a colitis risk gene that regulates stability of epithelial adherens junctions

Vishnu Mohanan,[1,2] Toru Nakata,[1,2] A. Nicole Desch,[1,2] Chloé Lévesque,[3] Angela Boroughs,[2] Gaelen Guzman,[1] Zhifang Cao,[2] Elizabeth Creasey,[2] Junmei Yao,[2] Gabrielle Boucher,[3] Guy Charron,[3] Atul K. Bhan,[4,5] Monica Schenone,[1] Steven A. Carr,[1] Hans-Christian Reinecker,[5,6] Mark J. Daly,[1,5,7] John D. Rioux,[3,8] Kara G. Lassen,[1,2]* Ramnik J. Xavier[1,2,5,6,9]*

Polymorphisms in *C1orf106* are associated with increased risk of inflammatory bowel disease (IBD). However, the function of C1orf106 and the consequences of disease-associated polymorphisms are unknown. Here we demonstrate that C1orf106 regulates adherens junction stability by regulating the degradation of cytohesin-1, a guanine nucleotide exchange factor that controls activation of ARF6. By limiting cytohesin-1–dependent ARF6 activation, C1orf106 stabilizes adherens junctions. Consistent with this model, *C1orf106*$^{-/-}$ mice exhibit defects in the intestinal epithelial cell barrier, a phenotype observed in IBD patients that confers increased susceptibility to intestinal pathogens. Furthermore, the IBD risk variant increases C1orf106 ubiquitination and turnover with consequent functional impairments. These findings delineate a mechanism by which a genetic polymorphism fine-tunes intestinal epithelial barrier integrity and elucidate a fundamental mechanism of cellular junctional control.

Intestinal epithelial cells are required for gut homeostasis and are involved in numerous physiologic processes including nutrient absorption, protection against microbes, and intestinal restoration following insult (*1*). Abnormal intestinal permeability has been observed in patients with inflammatory bowel disease (IBD), a chronic inflammatory condition of the gastrointestinal tract (*2*). Healthy family members of some IBD patients have been reported to have changes to the intestinal barrier, suggesting that host genetics can underlie cell-intrinsic barrier defects, although the underlying mechanisms are as yet undefined (*3*). *C1orf106* was identified as an IBD susceptibility gene through genome-wide association studies, and follow-up exome sequencing revealed that a coding variant in *C1orf106* (*333F) increased risk of IBD (*4*–*6*). Here we elucidate the function of C1orf106 and find a role for it in epithelial homeostasis. We report a mechanism whereby the *C1orf106* IBD-associated risk variant decreases cellular junctional integrity, suggesting a means by which this variant increases susceptibility to IBD.

C1orf106 is highly expressed in the human intestine and intestinal epithelial cell lines but expressed at low levels in myeloid cells and mouse bone marrow–derived macrophages (fig. S1, A to C). In Caco-2 cells, a human colorectal cell line, C1orf106 protein expression increased as cells differentiated and formed a polarized epithelial monolayer, a characteristic feature of the intestinal epithelium (Fig. 1A). To decipher the function of C1orf106, we sought to identify C1orf106-interacting proteins by tandem mass spectrometry–based affinity proteomics, using epitope-tagged C1orf106 immunoprecipitated from human embryonic kidney (HEK) 293T cells. Cytohesin-1 and cytohesin-2 were two of the top interactors (Fig. 1B, fig. S1D, and table S1). Cytohesin-1 is one of the guanine exchange factors (GEFs) that control the activation of ARF6 guanosine triphosphatase (GTPase) (*7*). Depending on the GEF involved, ARF6 functions to control the recycling of proteins from the plasma membrane (*8*). Coimmunoprecipitation experiments confirmed the interaction between C1orf106 and cytohesin-1 and -2 by overexpression in HEK293T cells and with endogenous proteins in Caco-2 cells (Fig. 1, C and D, and fig. S1E). Domain-mapping experiments further indicated that the N-terminal domain of C1orf106 interacts specifically with the N-terminal domain of cytohesin-1 (Fig. 1, C and E).

To investigate the functional interaction between these proteins in a physiologically relevant model, we generated *C1orf106*$^{-/-}$ mice (fig. S2, A and B) and examined the steady-state levels of cytohesin-1 in this model system. We found that cytohesin-1 protein levels in colon and small intestine epithelial cells isolated from *C1orf106*$^{-/-}$ mice were consistently increased 1.5- to 2-fold compared with those in cells isolated from *C1orf106*$^{+/+}$ mice (Fig. 1F). Consistent with these findings, *C1orf106*$^{-/-}$ epithelial monolayers derived from colonic organoids also exhibited increased levels of cytohesin-1 protein in both membrane and cytosolic protein fractions (Fig. 1G), despite no difference in cytohesin-1 mRNA levels (fig. S3A). These data suggest that the increase in cytohesin-1 is posttranscriptionally regulated and is not due to differential localization of the protein in the membrane versus in the cytoplasmic compartments of the cells. Consistent with this hypothesis, increasing C1orf106 expression significantly decreased the levels of either overexpressed or endogenous cytohesin-1, indicating that C1orf106 expression is sufficient to regulate the steady-state levels of cytohesin-1 (Fig. 1H and fig. S3B). Similar results were observed with cytohesin-2 (fig. S3C). These data suggest that expression of C1orf106 limits the steady-state levels of cytohesins.

We next investigated whether cytohesin-1 levels were regulated by ubiquitination and proteasomal degradation. Treatment of cells with MG132, a proteasome inhibitor, increased the steady-state levels of cytohesin-1, suggesting that cytohesin-1 is degraded by the proteasome (fig. S4A). Overexpression of C1orf106 was sufficient to increase the levels of ubiquitinated cytohesin-1 (Fig. 2A). Analysis of colonic intestinal epithelial cells demonstrated that *C1orf106*$^{-/-}$ cells have reduced levels of ubiquitinated cytohesin-1 at steady state (Fig. 2B). These data suggest a model whereby C1orf106 expression limits cytohesin-1 levels through ubiquitin-mediated degradation.

C1orf106 has one putative domain of unknown function, DUF3338, which is predicted to be involved in protein-protein interactions but lacks enzymatic activity. Therefore, we hypothesized that C1orf106 acts as a cofactor for ubiquitin ligases to ubiquitinate cytohesins. To understand the mechanism of C1orf106-mediated control of cytohesin-1 protein levels, we identified C1orf106-binding proteins in our proteomics data that have the potential to mediate ubiquitination. Importantly, each subunit of the SKP1–CUL1–F-box (SCF) E3 ubiquitin ligase complex and two F-box substrate adaptors, BTRC1 and FBXW11, were identified as C1orf106 interactors (Fig. 1B, fig. S1D, and table S1). SCF ubiquitin ligase complexes play important roles in regulating the ubiquitination and subsequent degradation of specific substrate proteins (*9*, *10*). We performed coimmunoprecipitation experiments to determine which proteins from the SCF complex interact specifically with C1orf106 (Fig. 2, C and D, and fig. S4, B and C); we found that the substrate adapters BTRC1 and FBXW11 do so, suggesting that C1orf106 may serve as a substrate cofactor (Fig. 2, C and D).

To test the hypothesis that the SCF complex mediates the ubiquitination of cytohesin-1, we knocked down expression of *BTRC1* and *FBXW11* and evaluated cytohesin-1 expression levels. Cells treated with *FBXW11* small interfering RNA (siRNA) showed significantly increased levels of cytohesin-1 (Fig. 2E and fig. S5), suggesting

[1]The Broad Institute of MIT and Harvard, Cambridge, MA 02142, USA. [2]Center for Computational and Integrative Biology, Massachusetts General Hospital, Boston, MA 02114, USA. [3]Montreal Heart Institute Research Center, Montreal, Quebec H1T 1C8, Canada. [4]Pathology Department, Massachusetts General Hospital and Harvard Medical School, Boston, MA 02114, USA. [5]Center for the Study of Inflammatory Bowel Disease, Massachusetts General Hospital, Boston, MA 02114, USA. [6]Gastrointestinal Unit, Massachusetts General Hospital, Boston, MA 02114, USA. [7]Analytic and Translational Genetics Unit, Massachusetts General Hospital and Harvard Medical School, Boston, MA 02114, USA. [8]Department of Medicine, Université de Montréal, Montreal, Quebec H1T 1C8, Canada. [9]Center for Microbiome Informatics and Therapeutics, Massachusetts Institute of Technology, Cambridge, MA 02139, USA.
*Corresponding author. Email: klassen@broadinstitute.org (K.G.L.); xavier@molbio.mgh.harvard.edu (R.J.X.)

that the SCF complex containing FBXW11, but not BTRC1, regulates the stability of cytohesin-1. We next tested the effect of MLN4924, a small-molecule inhibitor of a NEDD8-activating enzyme that is required for neddylation and activation of cullin-RING ubiquitin E3 ligases, including the SCF complex. Treatment of human colon HT-29 cells with MLN4924 resulted in a dose-dependent increase in endogenous levels of cytohesin-1 (Fig. 2F) (*11*). Taken together, these results indicate that cytohesin-1 levels are dynamically regulated by ubiquitination by the SCF ubiquitin ligase complex and subsequent proteasomal degradation.

We next sought to understand how C1orf106-mediated degradation of cytohesin-1 alters epithelial cell function. Cytohesin-1 acts as a GEF to regulate the activity of ARF6, a GTPase that controls the rate of membrane receptor recycling and mediates signaling pathways that control actin remodeling (*12*). We therefore hypothesized that increased levels of cytohesin-1 protein in *C1orf106*$^{-/-}$ cells would increase levels of ARF6 activation. To test this hypothesis, we evaluated the levels of activated ARF6 (ARF6-GTP) in organoid-derived intestinal epithelial monolayers, finding that ARF6-GTP levels were 1.5 times as high in *C1orf106*$^{-/-}$ cells as in *C1orf106*$^{+/+}$ cells, despite comparable total levels of ARF6 (Fig. 3A). Given that activated ARF6-GTP localizes to the plasma membrane (*8*), we next analyzed ARF6 localization in these cells. Immunostaining confirmed increased levels of ARF6 at the plasma membrane in *C1orf106*$^{-/-}$ epithelial monolayers (Fig. 3B). Analysis of insoluble membrane fractions from *C1orf106*$^{+/+}$ and *C1orf106*$^{-/-}$ epithelial monolayers demonstrated increased levels of ARF6 in the membrane fraction in *C1orf106*$^{-/-}$ cells, further supporting the finding of increased levels of membrane-associated ARF6-GTP in these cells (fig. S6A).

ARF6 plays a key role in regulating surface levels of critical adherens junction proteins, and ARF6 activation in epithelial cells is known to increase internalization of E-cadherin (*8*, *13*). We therefore hypothesized that increased cytohesin-1 and

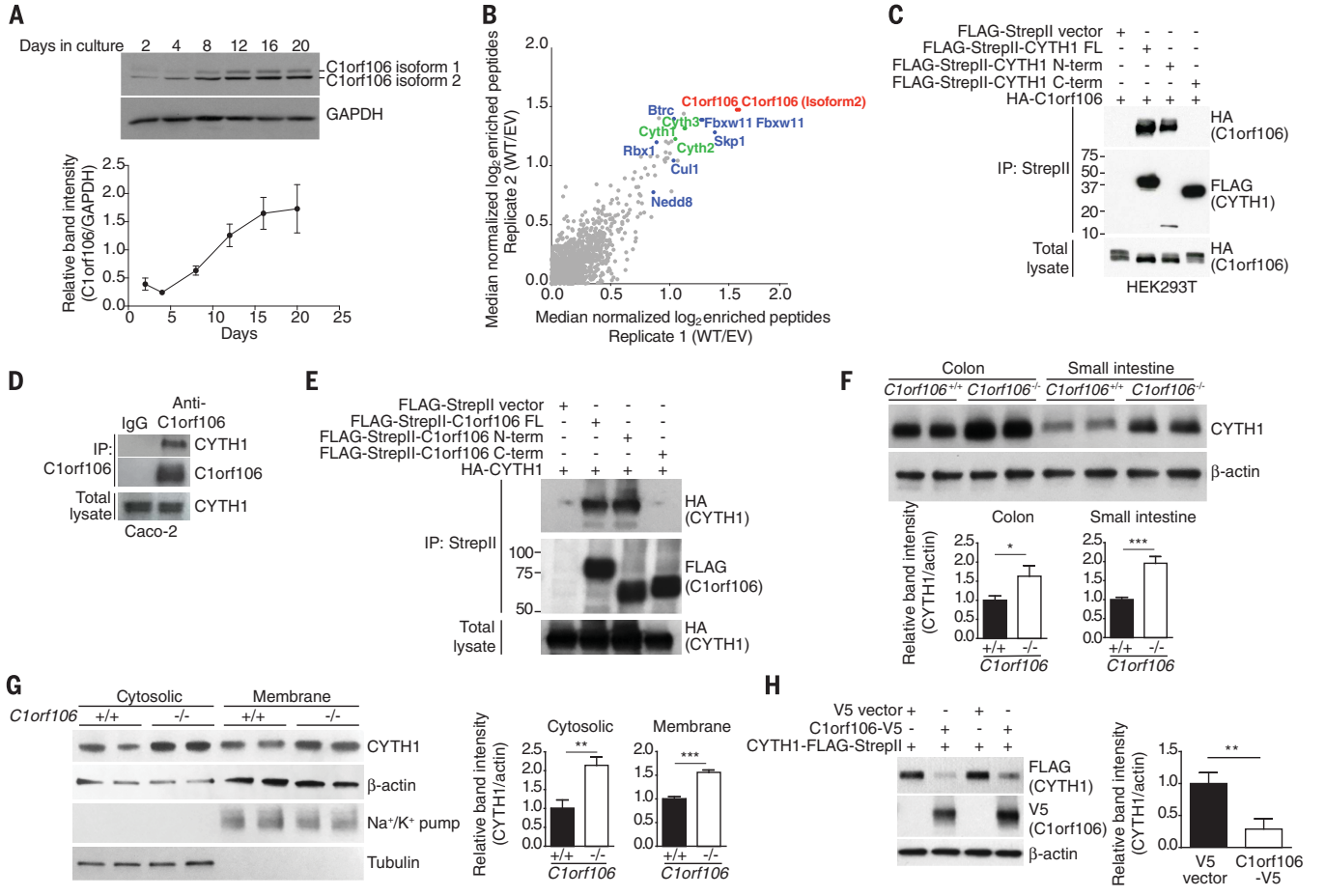

Fig. 1. C1orf106 modulates cytohesin-1 (CYTH1) levels. (**A**) C1orf106 protein levels were assessed during Caco-2 cell differentiation by immunoblot. Relative band intensity of C1orf106 isoform 1 at each time point was quantified and normalized to GAPDH (glyceraldehyde-3-phosphate dehydrogenase). Each value represents the mean of two independent experiments ± SEM. (**B**) Log_2 ratios of proteins enriched by FLAG antibody in HEK293T cells expressing FLAG-tagged C1orf106 (wild type, WT) to those enriched in cells transfected with an empty vector (EV); two replicates (one on each axis of the scatter plot) are shown. Each dot represents the log_2 ratio for a protein. Red dots, bait; blue dots, members of the SCF complex; green dots, cytohesins. (**C**) HEK293T cells were transiently transfected with HA (hemagglutinin)–C1orf106 and either empty vector, full-length (FL) FLAG-StrepII-CYTH1, or the N- or C-terminal domains of CYTH1 (Strep, streptavidin). Samples were immunoprecipitated (IP) with anti-StrepII and probed for FLAG (CYTH1) and HA (C1orf106). (**D**) Caco-2 cell lysates were immunoprecipitated with anti-IgG or anti-C1orf106 and probed for CYTH1 and C1orf106. (**E**) HEK293T cells were transiently transfected with HA-CYTH1 and either empty vector, full-length FLAG-StrepII-C1orf106, or the N- or C-terminal domains of C1orf106. Samples were immunoprecipitated with anti-StrepII and probed for FLAG (C1orf106) and HA (CYTH1). (**F**) Immunoblot analysis of intestinal epithelial cells isolated from the colon or small intestine of *C1orf106*$^{+/+}$ and *C1orf106*$^{-/-}$ mice. Shown are samples from individual mice. (**G**) Immunoblot analysis of monolayers grown from colonic organoids from *C1orf106*$^{+/+}$ and *C1orf106*$^{-/-}$ mice. (**H**) Immunoblot analysis of HEK293T cells cotransfected with CYTH1-FLAG-StrepII and empty vector or C1orf106-V5. Two biologic replicates are shown. In (F) to (H), graphs show normalized CYTH1:actin ratios from three independent experiments, as quantified by densitometry. Error bars, SD. *$P < 0.05$; **$P < 0.01$; ***$P < 0.001$ (two-tailed Student's *t* test).

ARF6-GTP levels in *C1orf106*$^{-/-}$ intestinal epithelial cells would result in decreased surface levels of E-cadherin. As predicted, immunostaining for E-cadherin in *C1orf106*$^{-/-}$ intestinal epithelial monolayers revealed more than a threefold increase in the proportion of cells containing intracellular E-cadherin puncta compared with the proportion among *C1orf106*$^{+/+}$ cells (Fig. 3C). An increase in intracellular E-cadherin puncta was also observed in colonic tissue sections from *C1orf106*$^{-/-}$ mice (Fig. 3D). We detected no differences in the localization of epithelial tight junction proteins occludin, ZO-1, claudin1, or claudin2 and no differences in mRNA or protein levels (Fig. 3, B to D, and fig. S6, B to E). These data confirm that the effect was specific for E-cadherin. The staining pattern of E-cadherin in *C1orf106*$^{-/-}$ colonic organoids was disorganized along the junctions and revealed increased puncta formation in the cytosol (fig. S6F). Moreover, disorganized E-cadherin was also observed after knockdown of *C1orf106* in differentiated human Caco-2 cells (fig. S6G). Additionally, internalized E-cadherin colocalized with intracellular ARF6 puncta, consistent with a role for ARF6 in E-cadherin internalization (fig. S7A). ARF6 is known to regulate actin dynamics. We observed prominent vesicular staining for actin along the inner cell membrane in *C1orf106*$^{-/-}$ cells, which further supports a role for altered ARF6 dynamics in these cells (fig. S7B). To confirm decreased localization of E-cadherin along the cell surface, we performed biotinylation of extracellular membrane-bound proteins followed by immunoblot analysis of biotinylated E-cadherin in freshly isolated colonic intestinal epithelial cells and organoid-derived monolayers from *C1orf106*$^{+/+}$ and *C1orf106*$^{-/-}$ mice. Despite similar total expression of E-cadherin, we found more than a twofold decrease in surface E-cadherin in *C1orf106*$^{-/-}$ cells compared with *C1orf106*$^{+/+}$ cells (Fig. 3, E and F). These data suggest a critical role for C1orf106 in maintaining adherens junctions by limiting ARF6 activation through regulated cytohesin degradation.

Epithelial junction integrity is important in intestinal homeostasis, as well as tissue repair after damage (*14*). We next monitored epithelial barrier integrity by testing the ability of fluorescently labeled molecules to pass through the intestinal barrier. *C1orf106*$^{-/-}$ and *C1orf106*$^{+/+}$ mice exhibited similar permeability to FITC (fluorescein isothiocyanate)–dextran (4 KDa) (Fig. 3G). However, *C1orf106*$^{-/-}$ colon tissue showed significantly increased permeability to a smaller compound, Lucifer yellow (0.4 KDa) (Fig. 3H). Together, these data suggest that loss of C1orf106 confers increased permeability to smaller solutes (*15*). To further confirm this finding, we measured transepithelial electrical resistance (TEER) to assess barrier function in *C1orf106*$^{+/+}$ and *C1orf106*$^{-/-}$ monolayers derived from organoids and Caco-2 cells with stable knockdown of *C1orf106*. Maximal TEER was significantly reduced in *C1orf106*-deficient cells compared with control cells, indicating impaired epithelial barrier integrity (fig. S8, A and B).

To test whether changes in E-cadherin recycling altered the ability of *C1orf106*$^{-/-}$ cells to repair epithelial junctions after injury, we subjected organoid-derived monolayers to a calcium switch assay by treating cells with EGTA to disrupt extracellular E-cadherin interactions, followed by treatment with normal media; in this assay, we monitored E-cadherin staining to evaluate the reformation of junctions after 2 hours of recovery time (*16*). Whereas both *C1orf106*$^{+/+}$ and *C1orf106*$^{-/-}$ monolayers were similarly disrupted by EGTA treatment, *C1orf106*$^{-/-}$ monolayers displayed a lack of reorganization compared with *C1orf106*$^{+/+}$ monolayers after 2 hours of recovery (fig. S8C). TEER was also measured after calcium switch during the recovery phase. *C1orf106*$^{-/-}$ monolayers displayed decreased TEER compared with *C1orf106*$^{+/+}$ monolayers at baseline and during the recovery phase (fig. S8D). Selective knockdown of cytohesin-1 was sufficient to rescue

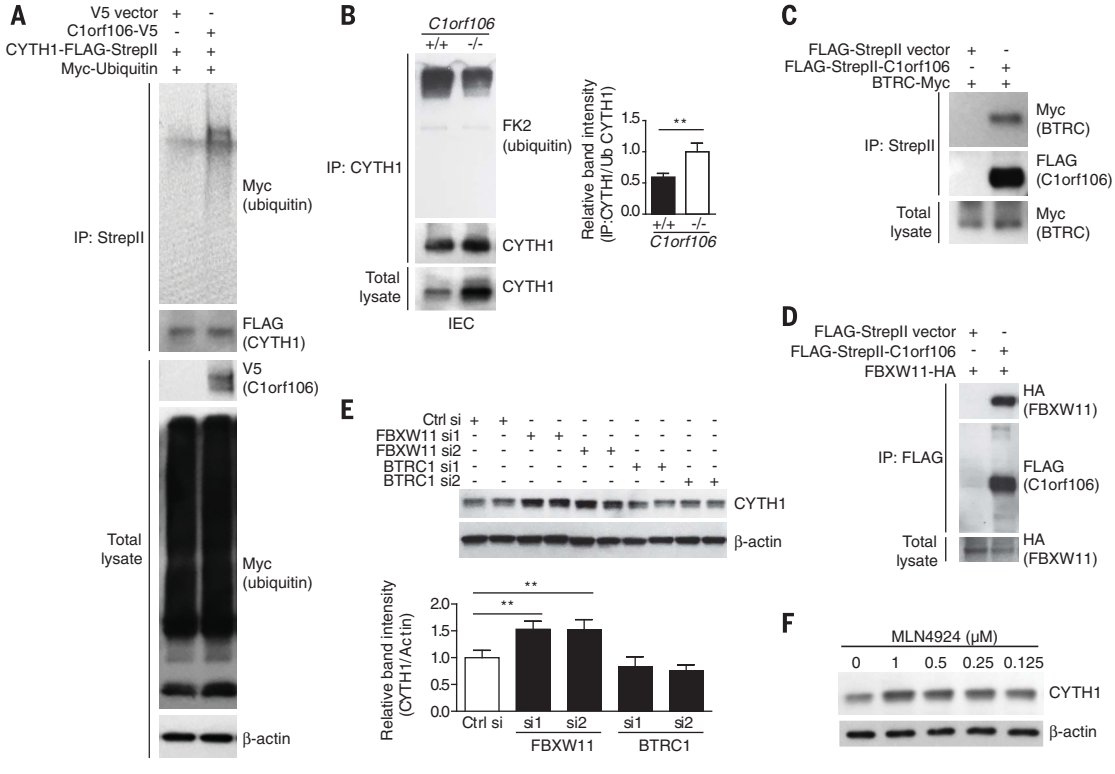

Fig. 2. C1orf106 regulates the ubiquitination of CYTH1 through the SCF ubiquitin ligase complex. (**A**) HEK293T cells were transfected with ubiquitin-Myc and CYTH1-FLAG-StrepII with or without C1orf106-V5. Samples were immunoprecipitated with anti-StrepII and probed for FLAG (CYTH1), V5 (C1orf106), and Myc (ubiquitin). (**B**) Endogenous CYTH1 was immunoprecipitated from *C1orf106*$^{+/+}$ and *C1orf106*$^{-/-}$ intestinal epithelial cell (IEC) monolayers and probed for CYTH1 and ubiquitin (FK2). The graph shows immunoprecipitated CYTH1:ubiquitinated CYTH1 ratios from three independent experiments, as quantified by densitometry. Error bars, SEM. $^{**}P < 0.01$ (two-tailed Student's *t* test). (**C**) HEK293T cells were transiently transfected with BTRC-Myc and either empty vector or full-length FLAG-StrepII-C1orf106. Samples were immunoprecipitated with anti-StrepII and probed for FLAG (C1orf106) and Myc (BTRC). (**D**) HEK293T cells were transfected with FLAG-StrepII-C1orf106 and FBXW11-HA and immunoprecipitated as in (C). (**E**) Immunoblot analysis of HEK293T cells transfected with siRNAs against BTRC or FBXW11 and probed for CYTH1. Samples from two biologic replicates are shown. The graph shows normalized CYTH1:actin ratios from three independent experiments, as quantified by densitometry. Error bars, SEM. $^{**}P < 0.01$ (two-tailed Student's *t* test). (**F**) Immunoblot analysis of HT-29 cells treated with DMSO (dimethyl sulfoxide) or MLN4924 and probed for CYTH1. Actin served as a loading control. Data are representative of three independent experiments.

baseline TEER in *C1orf106*$^{-/-}$ monolayers, demonstrating that cytohesin-1 is a key mediator of the observed barrier phenotype in *C1orf106*$^{-/-}$ cells (Fig. 3I and fig. S9, A and B).

In organoid-derived epithelial monolayers, *C1orf106*$^{-/-}$ cells had a significantly increased migratory rate at baseline and during hepatocyte growth factor–induced cell migration compared with *C1orf106*$^{+/+}$ cells (fig. S10). These findings suggest that loss of C1orf106 decreases junctional integrity, resulting in increased cellular migration at steady state, and that growth factor stimulation cannot compensate for this defect.

Increased susceptibility to microbial pathogens and dysbiosis is commonly associated with IBD (*17*). To determine whether *C1orf106*$^{-/-}$ mice have compromised epithelial barrier integrity resulting in increased bacterial dissemination, we challenged *C1orf106*$^{+/+}$ and *C1orf106*$^{-/-}$ mice with the extracellular intestinal murine pathogen *Citrobacter rodentium*, which induces colonic lesions, similarly to the clinical enteropathogenic *Escherichia coli* strains associated with Crohn's disease (*18*). Additionally, epithelial defenses are critical in limiting *C. rodentium* early after infection. *C1orf106*$^{-/-}$ mice exhibited significantly increased bacterial loads of *C. rodentium* at day 5 (Fig. 4A). Notably, translocation of *C. rodentium* to the mesenteric lymph nodes and spleen was also significantly increased in *C1orf106*$^{-/-}$ mice at day 5 (Fig. 4A). Although *C1orf106*$^{-/-}$ mice were able to control *C. rodentium* infection by day 12 postinfection, they exhibited significantly shortened colon length compared with *C1orf106*$^{+/+}$ mice and more severe histopathology, including crypt damage (Fig. 4, B to D, and fig. S11A). Cytokine response was not impaired in *C1orf106*$^{-/-}$ mice 12 days postinfection (fig. S11, B and C). Additionally, levels of immune cell types such as T and B lymphocytes, macrophages, dendritic cells, and innate lymphoid cells were unchanged at baseline (fig. S12A). Levels of interleukin-22, lipocalin-2, fecal immunoglobulin A (IgA), fecal albumin, and antimicrobial peptides were also unaltered at baseline, suggesting that these do

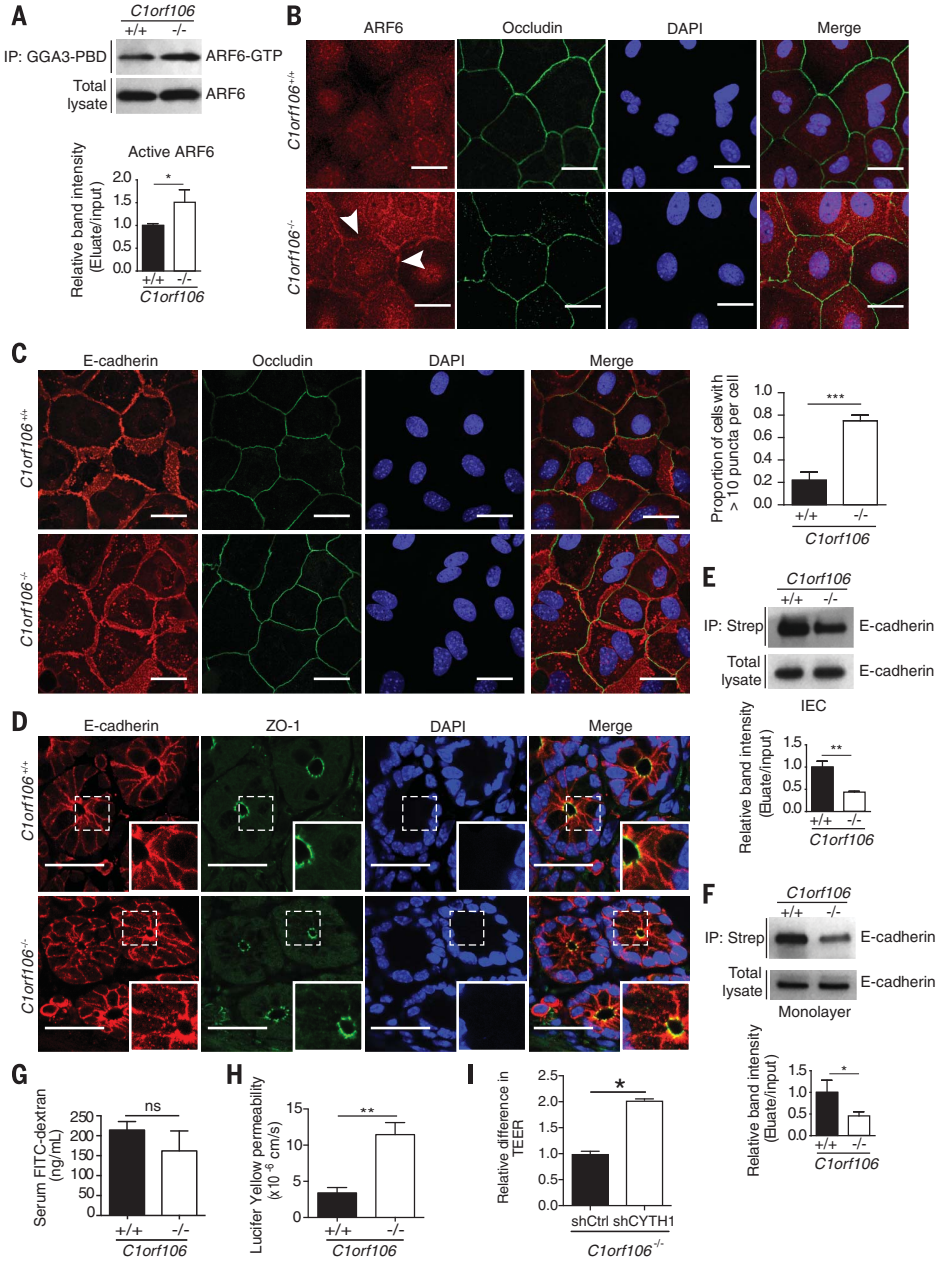

Fig. 3. C1orf106 controls surface E-cadherin levels through ARF6 activation. (**A**) IEC monolayers from *C1orf106*$^{+/+}$ and *C1orf106*$^{-/-}$ mice were immunoprecipitated with GGA3-PBD beads and probed with ARF6 antibody. Immunoblot is representative of three independent experiments. The graph shows total ARF6:ARF6-GTP ratios from three independent experiments, as quantified by densitometry. Error bars, SD. (**B**) Confocal images of colonic organoid–derived monolayers stained for ARF6, occludin, and nuclei (4′,6-diamidino-2-phenylindole, DAPI). Data are representative of three independent experiments. Arrowheads indicate ARF6 at the plasma membrane. Scale bars, 10 μm. (**C**) Confocal images of colonic organoid–derived monolayers stained for E-cadherin, occludin, and nuclei (DAPI). Scale bars, 30 μm. The graph shows quantification from three independent experiments of the percentage of cells that contained >10 intracellular E-cadherin puncta. Error bars, SEM. (**D**) Confocal immunofluorescence images of sections from *C1orf106*$^{+/+}$ and *C1orf106*$^{-/-}$ mouse colon stained for E-cadherin, ZO-1, and nuclei (DAPI). Scale bars, 30 μm. (**E** and **F**) Freshly isolated IECs (E) and organoid-derived monolayers (F) from *C1orf106*$^{+/+}$ and *C1orf106*$^{-/-}$ mice were biotinylated to label surface proteins and immunoprecipitated with streptavidin beads. Total lysate and immunoprecipitated lysate were probed for E-cadherin. Graphs show quantification from three independent experiments. Error bars, SD. (**G**) FITC-dextran levels in serum 3 hours postgavage in *C1orf106*$^{+/+}$ and *C1orf106*$^{-/-}$ mice. Error bars, SEM (n = 3 mice). Data are representative of three independent experiments. (**H**) Lucifer yellow permeability measurement from colon and small intestine epithelial tissues of *C1orf106*$^{+/+}$ and *C1orf106*$^{-/-}$ mice. Error bars, SEM from three independent experiments. (**I**) Relative difference in transepithelial electrical resistance (TEER) of colonic *C1orf106*$^{-/-}$ monolayers transduced with control vector (shCtrl) or shRNA against CYTH1 (shCYTH1) (sh, short hairpin). Data are representative of three independent experiments. Error bars, SEM. *P < 0.05; **P < 0.01; ***P < 0.001; ns, not significant [two-tailed Student's t test for (A), (C), and (E) to (I)].

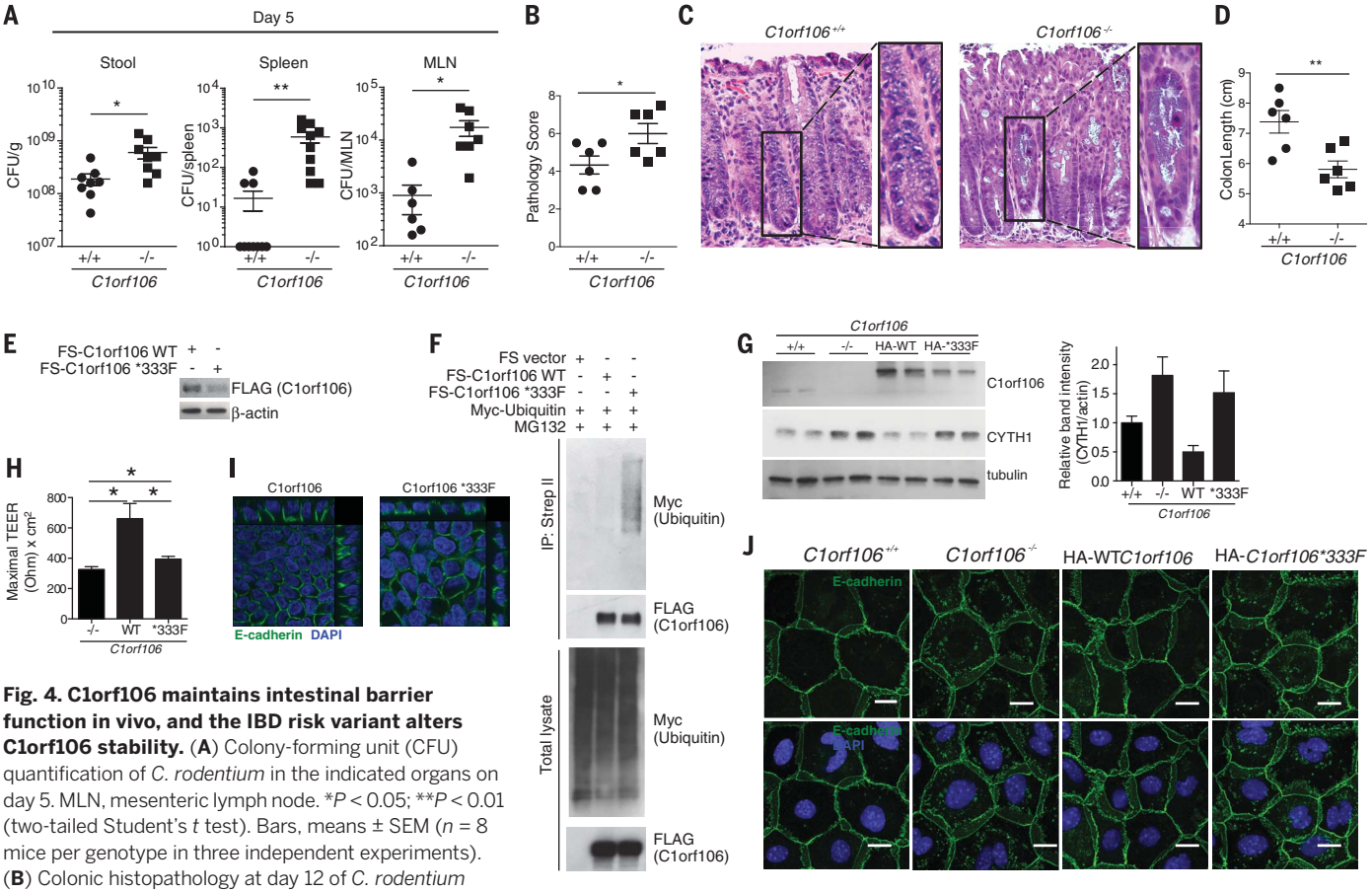

Fig. 4. C1orf106 maintains intestinal barrier function in vivo, and the IBD risk variant alters C1orf106 stability. (**A**) Colony-forming unit (CFU) quantification of *C. rodentium* in the indicated organs on day 5. MLN, mesenteric lymph node. $*P < 0.05$; $**P < 0.01$ (two-tailed Student's *t* test). Bars, means ± SEM ($n = 8$ mice per genotype in three independent experiments). (**B**) Colonic histopathology at day 12 of *C. rodentium* infection. $*P < 0.05$. Bars, means ± SEM ($n = 6$ mice per genotype in two independent experiments). (**C**) Representative hematoxylin and eosin–stained sections of colon from *C1orf106*$^{+/+}$ and *C1orf106*$^{-/-}$ mice infected for 5 days with *C. rodentium*. (**D**) Colon length from *C1orf106*$^{+/+}$ and *C1orf106*$^{-/-}$ mice at day 12 of *C. rodentium* infection. $**P < 0.01$ (Student's *t* test). Bars, means ± SEM ($n = 6$ mice per genotype in two independent experiments). (**E**) Immunoblot analysis of HEK293T cells transfected with FLAG–StrepII–C1orf106 WT or FLAG–StrepII–C1orf106 *333F (FS, FLAG-StrepII). (**F**) HEK293T cells were transfected with Myc-ubiquitin and either empty vector, FLAG–StrepII–C1orf106 WT, or FLAG–StrepII–C1orf106 *333F. Lysates from cells treated with 10 μM MG132 were immunoprecipitated with StrepII and probed for FLAG (C1orf106) and Myc (ubiquitin). (**G**) Immuboblot analysis of colonic *C1orf106*$^{+/+}$, *C1orf106*$^{-/-}$, HA–C1orf106 WT, and HA–C1orf106 *333F organoid-derived monolayers probed for C1orf106 or CYTH1. β-actin and tubulin served as loading controls. Error bars, SD. Data representative of three independent experiments. (**H**) Maximal TEER of monolayers from *C1orf106*$^{-/-}$, HA–C1orf106 WT, and HA–C1orf106 *333F organoids. $*P < 0.05$ (Student's *t* test). Error bars, SEM. Data are representative of at least three independent experiments. (**I**) Confocal immunofluorescence images (*XZ* and *YZ* planes) of LS174T cells stably overexpressing the indicated C1orf106 allele. Cells were stained for E-cadherin and nuclei (DAPI). (**J**) Confocal images of colonic organoid–derived monolayers from *C1orf106*$^{+/+}$, *C1orf106*$^{-/-}$, HA–C1orf106 WT, and HA–C1orf106 *333F, stained for E-cadherin and nuclei (DAPI). Scale bars, 10 μm.

not contribute to the early impairment in bacterial defense (fig. S12, B to F). *C1orf106*$^{-/-}$ mice also exhibited impaired recovery from dextran sodium sulfate–induced colitis, as evidenced by greater body weight loss, reduced colon length, and more severe histopathology, consistent with an impaired ability to recover from intestinal insults (fig. S13, A to D).

Deep exon sequencing has identified a coding variant in *C1orf106*, *333F, which is associated with increased risk of IBD. Expression of C1orf106 *333F was reproducibly decreased during transient transfection compared with that of wild-type C1orf106 (C1orf106 WT), despite comparable levels of mRNA, suggesting that the risk variant is poorly expressed or unstable (Fig. 4E and fig. S14A). To test whether the decreased levels of C1orf106 *333F protein were due to ubiquitination and degradation by the proteasome, we treated cells with MG132; treatment with this proteasome inhibitor restored C1orf106 *333F protein to WT levels (Fig. 4F). We also observed increased ubiquitination of C1orf106 *333F compared with WT, suggesting that the IBD risk polymorphism increases protein turnover of C1orf106, resulting in decreased expression of functional protein (Fig. 4F). Consistent with these results, we found that C1orf106 *333F had a half-life of 10.2 hours, compared with the C1orf106 WT half-life of almost 17 hours, using a cyclohexamide assay in LS174T cells (fig. S14B). To study the phenotypic effects of the decreased half-life of C1orf106 *333F, *C1orf106*$^{-/-}$ organoids were transduced with either C1orf106 WT or C1orf106 *333F. Expression of C1orf106 *333F was not sufficient to restore WT levels of C1orf106, mediate degradation of cytohesin-1, or increase the TEER in *C1orf106*$^{-/-}$ monolayers (Fig. 4, G and H). Expression of C1orf106 *333F disrupted E-cadherin and actin organization and staining in monolayer-derived intestinal epithelial cells and human intestinal cells (Fig. 4, I and J, and fig. S15). Taken together, these data suggest a mechanism by which the *333F polymorphism decreases C1orf106 protein stability and thus confers increased susceptibility to IBD by compromising gut epithelial integrity through impaired turnover and degradation of cytohesin-1.

Our findings define a critical function for C1orf106 in IBD by regulating the integrity of intestinal epithelial cells. We have shown that C1orf106 functions as a molecular rheostat to limit cytohesin levels through SCF complex–dependent degradation and thereby modulates

barrier integrity. The finding that C1orf106 regulates the surface levels of E-cadherin is notable given that polymorphisms in both *C1orf106* and *CDH1* (E-cadherin) are associated with increased risk of ulcerative colitis, a form of IBD (*19*). Increasing the stability of C1orf106 may be a potential therapeutic strategy to increase the integrity of the epithelial barrier for the treatment of IBD.

REFERENCES AND NOTES

1. B. Khor, A. Gardet, R. J. Xavier, *Nature* **474**, 307–317 (2011).
2. J. Mankertz, J. D. Schulzke, *Curr. Opin. Gastroenterol.* **23**, 379–383 (2007).
3. D. Hollander *et al*., *Ann. Intern. Med.* **105**, 883–885 (1986).
4. C. A. Anderson *et al*., *Nat. Genet.* **43**, 246–252 (2011).
5. M. A. Rivas *et al*., *Nat. Genet.* **43**, 1066–1073 (2011).
6. Y. Liu *et al*., *PLOS Genet.* **7**, e1001338 (2011).
7. J. E. Casanova, *Traffic* **8**, 1476–1485 (2007).
8. J. G. Donaldson, C. L. Jackson, *Nat. Rev. Mol. Cell Biol.* **12**, 362–375 (2011).
9. D. Frescas, M. Pagano, *Nat. Rev. Cancer* **8**, 438–449 (2008).
10. J. R. Skaar, J. K. Pagan, M. Pagano, *Nat. Rev. Mol. Cell Biol.* **14**, 369–381 (2013).
11. T. A. Soucy *et al*., *Nature* **458**, 732–736 (2009).
12. W. Kolanus, *Immunol. Rev.* **218**, 102–113 (2007).
13. F. Palacios, L. Price, J. Schweitzer, J. G. Collard, C. D'Souza-Schorey, *EMBO J.* **20**, 4973–4986 (2001).
14. T. J. Harris, U. Tepass, *Nat. Rev. Mol. Cell Biol.* **11**, 502–514 (2010).
15. L. Shen, C. R. Weber, D. R. Raleigh, D. Yu, J. R. Turner, *Annu. Rev. Physiol.* **73**, 283–309 (2011).
16. G. Swaminathan, C. A. Cartwright, *Oncogene* **31**, 376–389 (2012).
17. D. Knights, K. G. Lassen, R. J. Xavier, *Gut* **62**, 1505–1510 (2013).
18. S. Nell, S. Suerbaum, C. Josenhans, *Nat. Rev. Microbiol.* **8**, 564–577 (2010).
19. UK IBD Genetics Consortium, Wellcome Trust Case Control Consortium 2, *Nat. Genet.* **41**, 1330–1334 (2009).

ACKNOWLEDGMENTS

We thank the members of the Xavier laboratory for helpful discussions, N. Nedelsky and T. Reimels for editorial and graphics assistance, and J. Rush for comments. We thank the Center for Celiac Research and Treatment for their assistance with the intestinal permeability experiment. **Funding:** This work was supported by funding from the Crohn's & Colitis Foundation, funded by a generous anonymous donor; the Helmsley Charitable Trust; and National Institutes of Health (NIH) grants DK043351, AI109725, and DK062432 to R.J.X. H.–C.R. was supported by NIH grants AI113333, DK068181, DK091247, and DK043351. J.D.R. holds a Canada Research Chair, and this work was supported by NIH grant DK064869 to J.D.R. This project also benefited from infrastructure supported by the Canada Foundation for Innovation (grants 202695, 218944, and 20415; J.D.R.). **Author contributions:** V.M., G.G., A.B., A.N.D., C.L., G.B., G.C., T.N., E.C., J.Y., and Z.C. performed experiments. V.M., M.S., G.G., A.B., A.N.D., C.L., G.B., G.C., T.N., and A.K.B. analyzed data. V.M., M.S., M.D., A.N.D., C.L., G.B., G.C., H–C.R., T.N., J.D.R., K.G.L., and R.J.X. designed the research. V.M., M.S., S.A.C., M.J.D., H–C.R., J.D.R., K.G.L., and R.J.X. provided intellectual contributions throughout the project. V.M., R.J.X., and K.G.L. wrote the paper. **Competing interests**: The authors declare no competing financial interests. **Data and materials availability:** Data in this paper are tabulated in the main text and supplementary materials. The original mass spectra can be downloaded from MassIVE (Mass Spectrometry Interactive Virtual Environment; http://massive.ucsd.edu) using the identifier MSV000081941. The data are directly accessible at ftp://massive.ucsd.edu/MSV000081941.

SUPPLEMENTARY MATERIALS

www.sciencemag.org/content/359/6380/1161/suppl/DC1
Materials and Methods
Figs. S1 to S15
Table S1
References (*20*–*28*)

1 March 2017; resubmitted 1 October 2017
Accepted 21 January 2018
Published online 1 February 2018
10.1126/science.aan0814

Science

C1orf106 is a colitis risk gene that regulates stability of epithelial adherens junctions

Vishnu Mohanan, Toru Nakata, A. Nicole Desch, Chloé Lévesque, Angela Boroughs, Gaelen Guzman, Zhifang Cao, Elizabeth Creasey, Junmei Yao, Gabrielle Boucher, Guy Charron, Atul K. Bhan, Monica Schenone, Steven A. Carr, Hans-Christian Reinecker, Mark J. Daly, John D. Rioux, Kara G. Lassen and Ramnik J. Xavier

Science **359** (6380), 1161-1166.
DOI: 10.1126/science.aan0814originally published online February 1, 2018

Overcoming a barrier to IBD

Inflammatory bowel disease (IBD) is a group of disorders linked to inflammation of the gastrointestinal tract. Colitis is a type of IBD that affects the inner lining of the colon and has been linked to a gene known as *C1orf106*. Mohanan *et al.* found that *C1orf106* encodes a protein that stabilizes the integrity of epithelial junctions and enhances barrier defense (see the Perspective by Citi). IBD-associated mutations in *C1orf106* lead to greater cytohesin-1 protein levels, changes in E-cadherin localization, and enhanced susceptibility to intestinal pathogens. Modulation of C1orf106 may thus hold promise for treating colitis and other IBDs.

Science, this issue p. 1161; see also p. 1097